

Parkinson's Disease Detection with Ensemble Architectures based on ILSVRC Models

Tahjid Ashfaque Mostafa
Department of Computing Science
University of Alberta
Edmonton, Canada
tahjid@ualberta.ca

Irene Cheng
Department of Computing Science
University of Alberta
Edmonton, Canada
locheng@ualberta.ca

Abstract—In this work, we explore various neural network architectures using Magnetic Resonance (MR) T1 images of the brain to identify Parkinson's Disease (PD), which is one of the most common neurodegenerative and movement disorders. We propose three ensemble architectures combining some winning Convolutional Neural Network models of ImageNet Large Scale Visual Recognition Challenge (ILSVRC). All of our proposed architectures outperform existing approaches to detect PD from MR images, achieving upto 95% detection accuracy. We also find that when we construct our ensemble architecture using models pretrained on the ImageNet dataset unrelated to PD, the detection performance is significantly better compared to models without any prior training. Our finding suggests a promising direction when no or insufficient training data is available.

I. INTRODUCTION

In recent years, Computer aided diagnosis systems based on brain imaging have shown merits in the diagnosis of Parkinson's Disease (PD), with the objective to detect PD by automatic recognition of patterns that characterize it. PD is the second most common neurodegenerative disorder and the most common movement disorder affecting the elderly next to the Alzheimer's disease [1]. The root cause of PD is thought to be the loss of nerve cells (neurons) in Substantia Nigra part of Basal Ganglia, which is one of the major regions of the human brain located deep within the cerebrum, below cerebral cortex. Dopamine, the neurotransmitter of the brain, is produced in this region, which facilitates the communication between neurons. This communication is essential for coordination of body movement and a shortage of dopamine hampers it, leading to PD.

PD has been associated with neurological symptoms like speech impediments, olfactory dysfunctions, sleep disorders, autonomic dysfunctions, fatigue and balance issues like tremors, Bradykinesia, postural instability, rigidity of the limbs, impaired gait etc. It has been clinically studied and defined for a long time, but the exact mechanisms leading to PD are still not properly identified [3]. In majority of the cases, PD is diagnosed with the manifestation of motor symptoms. But these symptoms might not become apparent until 50 to 70% of neurons have been damaged [4], which is too late for any sort of preventive measures. Even though a guaranteed cure for PD has not been discovered yet, early detection might offer an opportunity for slowing or stopping the progression

of the disease. There are also new forms of treatment like Exenatide [7], which show promising results with cases where PD was detected in the initial stages.

One of the techniques that has been found to be successful in detecting neurodegenerative diseases with cognitive impairments [5] [6] is the analysis of the structural changes in the brain using Medical Imaging techniques. Specifically, Magnetic Resonance (MR) images, which possess high contrast and resolution within soft tissue have been found to provide better performance in brain structure analysis.

In this work, we propose three ensemble architectures to identify PD from MR images of the brain and analyze whether models pre-trained on unrelated ImageNet [30] dataset perform better than models without any prior training in detecting PD. We achieve over 90% detection accuracy for all three of our architectures with the highest being 95.15%, which is better than existing models using similar data. We also found that using models pretrained on the ImageNet dataset to construct our ensemble architecture yields much better performance than using untrained models, even though the training data is unrelated to PD.

II. BACKGROUND AND RELATED WORKS

A multitude of Machine Learning (ML) [3], [8]–[10] and Deep Learning (DL) [11], [13] based approaches have been introduced for the detection of Parkinson's Disease. Focke et al. [8] extracted Gray Matter (GM) and White Matter (WM) from MR images and fed them to a SVM Classifier for PD detection achieving 39.53% and 41.86% classification accuracy for GM and WM respectively. Radial Basis Function Neural Network (RBFNN) was used by Pazhanirajan et al. [9] for PD classification. Babu et al. [12] achieved a 87.21% accuracy in classifying PD using GM with a Computer Aided Diagnosis (CAD) system. They identified Superior Temporal Gyrus as a potential biomarker which plays a vital role for PD.

Choi et al. [11] achieved an accuracy of 96% using SPECT imaging with Convolutional Neural Network [CNN]. Although their accuracy was very high, SPECT Imaging is invasive and not very popular as it requires injecting a radioactive tracer into the patient. Around 100 times more MRI scans were performed compared to SPECT over one year period in the

NHS operation in England. Thus the SPECT approach seems to be impractical for normal medical use due to limited sample size, despite its reported high accuracy. The dataset is also class imbalanced since about 69% of the data is from PD patients. Class imbalance causes the models to over classify the majority class [15].

To detect PD from resting-state functional MRI (rsf-MRI), which detects subtle changes in blood oxygenation level, whereas Structural MRI (sMRI) only captures the anatomical details and ignores all activity, Long et al. [16] used a ML based approach and they achieved 87% classification accuracy, but the dataset used by them was very small. Rana et al. [18] used a SVM for classification with t-test feature selection on WM, GM and Cerebrospinal Fluid (CSF) achieving 86.67% accuracy for GM and WM and 83.33% accuracy for CSF. In another work [19], the authors used the relation between tissues instead of considering the tissues separately and achieved an accuracy of 89.67%.

Among the various regions in the brain, the Substantia Nigra (SN) region has significant correlation with PD according to Braaks neuroanatomical model of Parkinsons Disease [17] and it is often used as a Region Of Interest (ROI) in PD identification. But we will not be using this region of the brain for our analysis, instead we consider GM and WM only, since we found that the detection accuracy increased drastically using GM and WM in our previous work [36].

ImageNet [30] is one of the well known image datasets for computer vision. It is unrelated to PD detection. ImageNet is organized according to the WordNet [37], [38] hierarchy. WordNet is one of the largest lexical database of English words with nouns, verb, adjectives etc organised into "synonym sets" or "synsets", which are sets of cognitive synonyms. A "synset" describes a meaningful concept with multiple words or word phrases. WordNet contains more than 100,000 synsets, with more than 80,000 being nouns. Currently ImageNet labels images using only the nouns from WordNet. Each node of WordNet hierarchy is represented by thousand image samples in ImageNet on average. The ImageNet Large Scale Visual Recognition Challenge(ILSVRC) [31] evaluates the performance of various algorithms for object detection and image classification on the ImageNet dataset. The challenge has 1000 object categories, with the categories containing both internal and leaf nodes of ImageNet, but they do not overlap. Fig. 1 shows two sample images from the ImageNet dataset and their positions in the WordNet hierarchy. Kornblith et al. [35] proposed that models performing well on the ILSVRC also perform better when they are applied on other datasets. In our previous work [36], we tried a combination of multiple neural networks trained on PD data to create ensemble architectures for detecting PD, as shown in Fig. 2. In this work, we built ensemble architectures, composed of ILSVRC models pretrained using non-PD related ImageNet images. We then used MR images to validate the effectiveness of these architectures. We separated WM and GM from MR scans of the brain and passed them through our architectures. Experimental results showed that when using GM and WM,



(a) Animal-Beast-Chordate-Vertebrate-Mammal-Placental-Carnivore-Feline-Big Cat-Lion



(b) Artifact-Instrumentation-Container-Wheeled Vehicle-Self Propelled Vehicle-Motor Vehicle-Car/Automobile-Race Car

Fig. 1. Sample Images from ImageNet [30] dataset and their position in the WordNet [37], [38] Hierarchy

ensemble architectures with models pretrained on ImageNet data achieve better performance in detecting PD.

The objectives of this paper are two-folds, (1) We want to know whether Kornblith's hypotheses and our observation from previous work holds true if we transfer those models learnt on completely unrelated data to detect PD. (2) The detection accuracy using sMRI was lacking in current methods and none of the methods we looked into were using ensemble architectures for PD detection. We want to demonstrate that creating ensemble architectures combining different characteristics of deep learning models has potential to give us better results. Our approach is described in the next section.

III. PROPOSED METHOD

A. Data

We used Parkinson Progression Markers Initiative (PPMI) dataset [20] for our experiments, which consists of T1-weighted sMRI scans for 568 PD and Healthy Control(HC) subjects. We only chose 445 subjects and discarded the rest due to structural anomalies during preprocessing steps. There was a class imbalance in the resulting data with 299 PD and 146 HC subjects. To balance the data, we collected 153 HC T1-weighted sMRI scans from the publicly available IXI dataset [21]. The final dataset was class balanced with 598

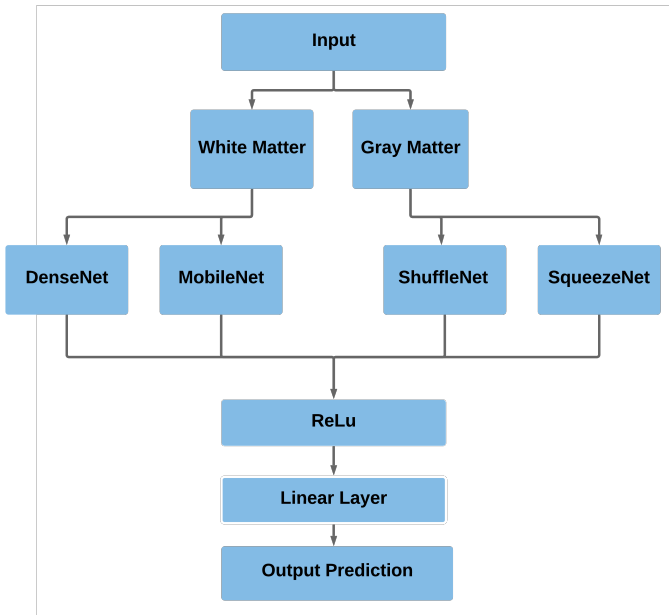


Fig. 2. Ensemble architecture from previous experiment [36]

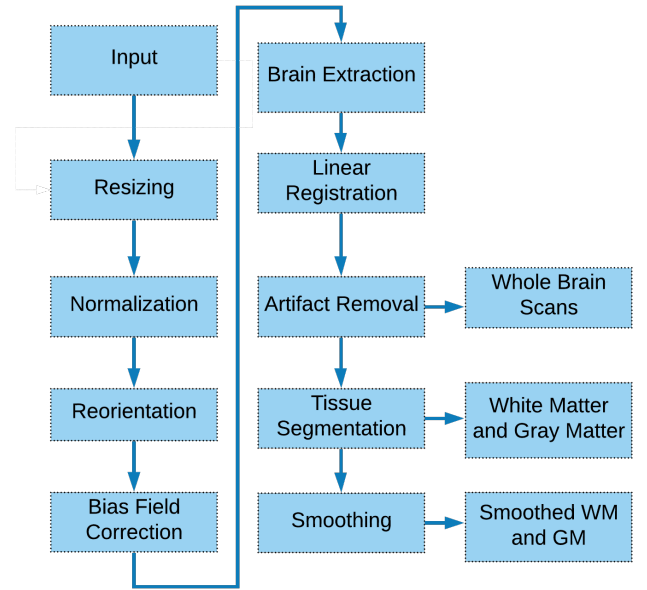


Fig. 3. Preprocessing Pipeline

subjects. The demographic for the dataset is presented in Table I.

TABLE I
DEMOGRAPHIC DATA

	PD	HC	Average
Age(Years)	62.0 ± 9.54	49.2 ± 16.9	55.6 ± 15.1
Sex (Male / Female)	189 / 110	172 / 127	361 / 237

B. Preprocessing

The scans we had come from different machines, so there were dimensional and morphological disparities between the data. We had to standardize the data to a common format to make it comparable. All scans were resized to the same dimensions. For preprocessing, Statistical Parameter Mapping (SPM12) [22], [23] and Computational AnatomToolbox (CAT12) [24] were used.

The structure of our preprocessing pipeline is presented in Fig. 3. Since MRI intensity varies from subject to subject, to minimize discrepancies we normalize the values to a [0,1] range. After that the images were aligned to a standard space named Montreal Neurological Institute (MNI) and general intensity non-uniformities are removed using bias field correction (FAST) [26]. FNIRT / BET [27] was used to extract brain from the scans. The skull, fat and background regions which do not contain useful information were removed. The data was registered to MNI152 format (FLIRT) [28], [29]. After that artifact removal was performed, i.e. any voxel intensity values higher than 1 was corrected to be in the range [0,1]. Then a deformation method was applied to extract Gray Matter (GM) and White Matter (WM) from the scan and a 8mm Isotropic Gaussian Kernel was used to smooth and increase the signal-to-noise ratio and remove unnecessary

portions of the scan. Finally we have three separate datasets: whole brain scans, GM and WM extracted from the brain and Smoothed GM and WM. Examples of the extracted brain and the resultant WM and GM extracted from the brain are given in Fig. 4. For our experiments, we did not use the whole brain scans, which produced less promising results based on our earlier analysis [36]. Our models were designed to handle the extracted WM and GM scans and the smoothed version of WM and GM scans.

C. Model Architecture

We created three separate ensemble architectures combining existing model architectures of the ILSVRC [31] implemented in Pytorch [33]. We selected 6 models to construct our ensemble architectures and choose the three architectures with better performances:

- ResNet 101 [39]
- SqueezeNet 1.1 [40]
- DenseNet 201 [41]
- VGG 19 [42]
- MobileNet V2 [43]
- ShuffleNet V2 [44]

These models are available from Torchvision [34] in two versions: without any kind of training (untrained) and trained on the ImageNet dataset. We used both untrained and pretrained models to construct our ensemble networks and compared the performances of the resultant architectures to examine if training on the unrelated Imagenet dataset makes the models perform better in PD identification. Since the models were designed with the ImageNet dataset in mind, we had to modify the models in order to accommodate the format of MRI data. The input layers of all models were changed to accommodate

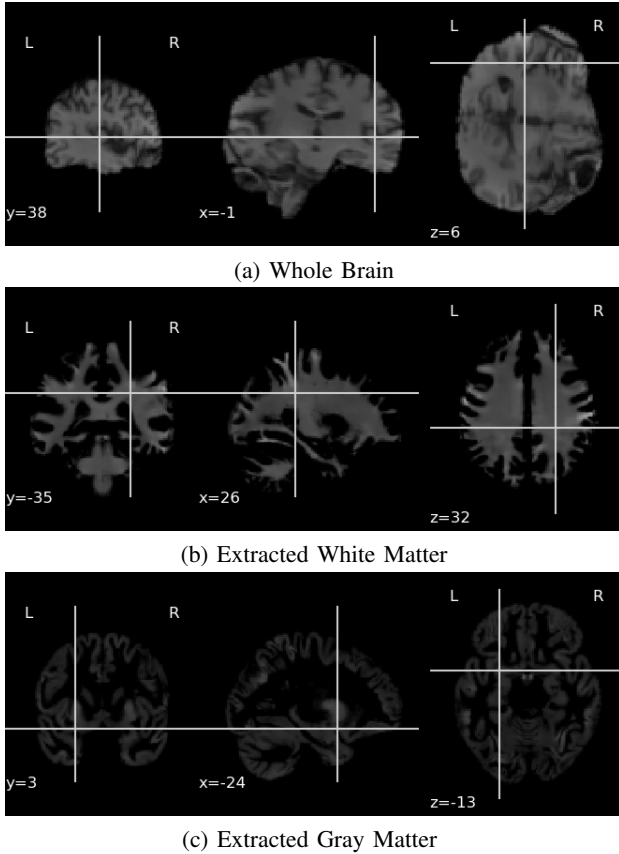


Fig. 4. Sample MRI scans for a Healthy Control Patient and the extracted GM and WM

the format of our input and the output layers were changed to predict between 2 classes (PD and HC) instead of the 1000 ImageNet classes.

D. Core Architecture

For our main architecture, we take the extracted GM and WM scans dimension $121 \times 145 \times 121$ and pass them in parallel through two blocks comprised of multiple ILSVRC models as described above. We refer to this combination of models as a Model Block. We then concatenate the output from both blocks and then pass them through a ReLU activation layer and then through a final linear layer which predicts between the two output classes. Fig. 5 shows a visual representation of this architecture. We used multiple combinations of models to create different versions of Model Block, replaced them in the core architecture and tested their performances with both pretrained and untrained models.

1) *Architecture 1*: The model block was comprised of DenseNet, ShuffleNet and SqueezeNet in parallel. The input was passed through all three models simultaneously, as shown in Fig. 6.

2) *Architecture 2*: The model block was created by adding MobileNet to Block 1, so it was comprised of DenseNet, ShuffleNet, SqueezeNet and MobileNet in parallel. The input was passed through all four models simultaneously, as shown in Fig. 7.

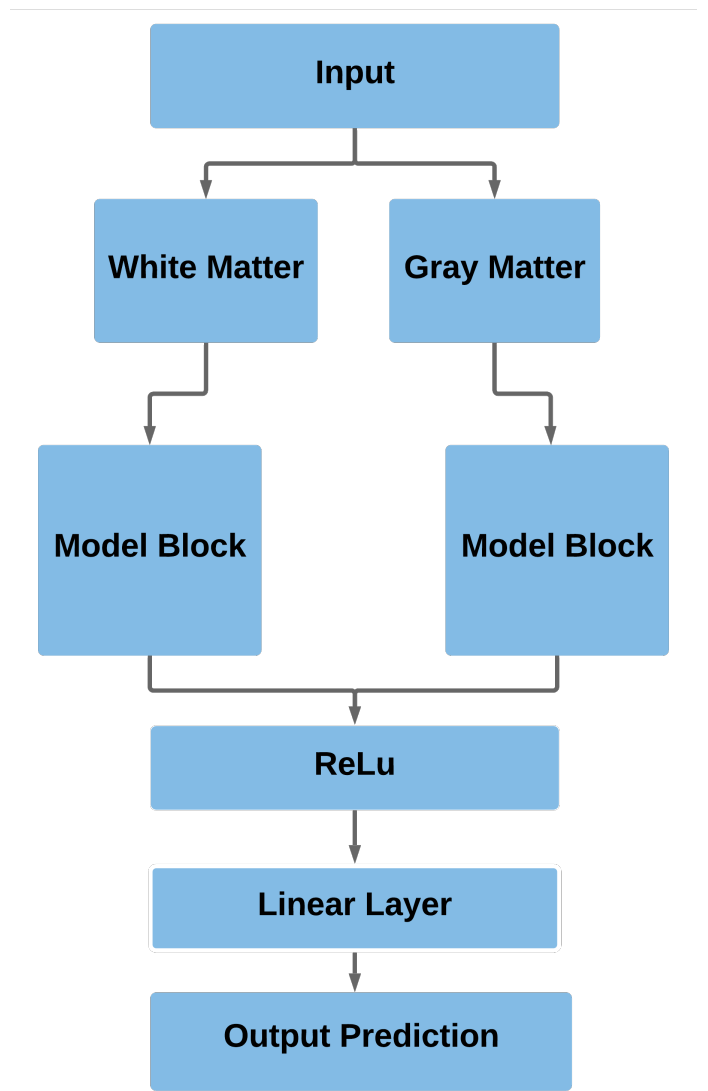


Fig. 5. Core Architecture

3) *Architecture 3*: The model block was created with ShuffleNet, VGG and MobileNet in parallel. The input was passed through all three models simultaneously, as shown in Fig. 8

IV. EXPERIMENTAL RESULTS

We created 2 separate versions for each of our ensemble architectures; one with all untrained constituent models and another with all pretrained constituent models. The dataset was randomly split and 80% was selected for training and 20% for testing. Each model was trained for 25 epochs with an Adam Optimizer. We used Cross Entropy Loss function. At each epoch, the training set was further split randomly and 20% was selected for validation. We used a learning rate of **.001** and **.0001**. We repeated the process multiple times and the average results are presented in Table II along with the results of some other approaches on similar data.

TABLE II
RESULTS

Model	Use Smoothed Scan	Pre Trained	Learning Rate	Classification Accuracy (On a scale of 0-1)
Architecture 1	False	False	.001	0.6045
			.0001	0.8097
		True	.001	0.9291
			.0001	0.8955
	True	False	.001	0.7303
			.0001	0.6592
		True	.001	0.8315
			.0001	0.7528
Architecture 2	False	False	.001	0.5485
			.0001	0.7276
		True	.001	0.9515
			.0001	0.9440
	True	False	.001	0.5768
			.0001	0.7416
		True	.001	0.8614
			.0001	0.8352
Architecture 3	False	False	.001	0.5187
			.0001	0.5522
		True	.001	0.9029
			.0001	0.9254
	True	False	.001	0.5805
			.0001	0.6105
		True	.001	0.8914
			.0001	0.8390
Our Previous Result [36] using extracted GM and WM Scans	False	False	.001	0.5487 ± 0.0002
			.0001	0.6847 ± 0.0093
		True	.001	0.9231 ± 0.0258
			.0001	0.9366 ± 0.0170
	True	False	.001	0.5410 ± 0.0106
			.0001	0.7276 ± 0.0476
		True	.001	0.9291 ± 0.0170
			.0001	0.9470 ± 0.0083
Focke et al. [8] [GM]	N/A	N/A	N/A	0.3953
Focke et al. [8] [WM]	N/A	N/A	N/A	0.4186
Babu et al. [12] [GM]	N/A	N/A	N/A	0.8721
Rana et al. [18] [GM & WM]	N/A	N/A	N/A	0.8667
Rana et al. [19]	N/A	N/A	N/A	0.8967

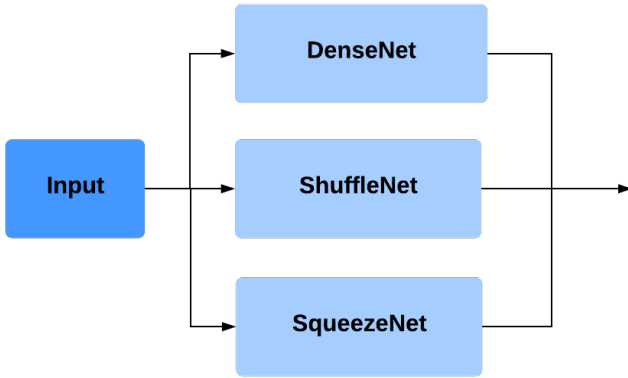


Fig. 6. Architecture 1 Model Block

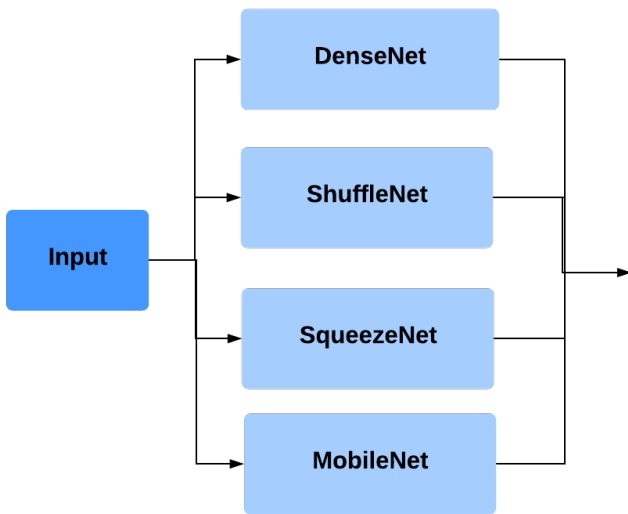


Fig. 7. Architecture 2 Model Block

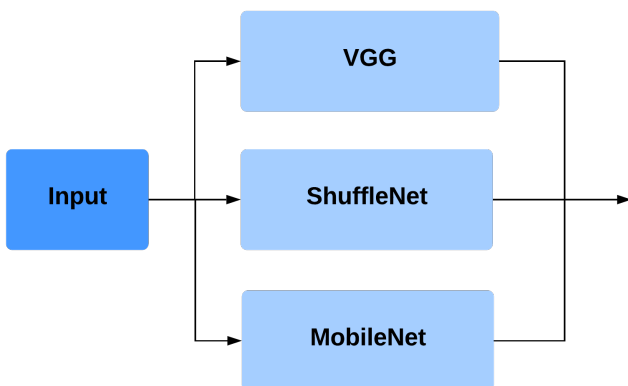


Fig. 8. Architecture 3 Model Block

For all three different architectures, we can see that the accuracy increases significantly when we use pretrained models to construct the model blocks. For Architecture 1, the accuracy we achieved was 0.9291 with non smoothed scans with a learning rate of 0.001. For Architecture 2, we achieved a detection accuracy of 0.9515 for non smooth scans with 0.001 learning rate, which was the best overall accuracy we achieved in our experiments. Architecture 3 achieved an accuracy of 0.9254 for non smooth scans and a learning rate of 0.0001. All three of our architectures perform better than existing models on similar data and achieve above 90% accuracy. For comparison, we also present our results from our earlier finding [36] where pretrained models provide higher detection accuracy as well. We note that we achieved better accuracy than our previous work with an architecture constructed with pretrained models and non smoothed scans. It is also noted that the smoothing process actually caused reduced detection accuracy in our experiments with these architectures.

V. CONCLUSION AND FUTURE WORKS

In this paper, we proposed three novel Ensemble architectures for Parkinson's Disease Detection, which outperform related works on similar dataset and achieve considerable detection accuracy of around 95.15%. We also find that, when we used models pretrained on unrelated ImageNet dataset for the construction of the ensemble architectures, it significantly enhanced the performance on detecting PD compared to untrained models. Our finding suggests a promising direction, where unrelated training data can be considered when insufficient or no training data is available for a particular application.

Our next step will be to analyse the decision making process of our model, perform occlusion analysis to see which region of the scans our models use to make the decisions and use the Substantia Nigra as the target of significance to assess if it produces better results than using GM and WM regions.

ACKNOWLEDGMENT

Special thanks to PPMI for supporting Parkinsons disease research by maintaining and updating their clinical dataset.

Data used in the preparation of this article were obtained from the Parkinsons Progression Markers Initiative (PPMI) database (www.ppmi-info.org/data). For up-to-date information on the study, visit www.ppmi-info.org.

PPMI is a public-private partnership funded by the Michael J. Fox Foundation for Parkinsons Research and other funding partners listed at www.ppmi-info.org/fundingpartners.

Special thanks for the advice from Dr. Sara Soltaninejad (soltanin@ualberta.ca), previous PhD student at the Department of Computing Science, University of Alberta.

Financial support from the Natural Sciences and Engineering Research Council of Canada (NSERC) is gratefully acknowledged.

REFERENCES

- [1] Mhyre T.R., Boyd J.T., Hamill R.W., Maguire-Zeiss K. (2012) Parkinsons Disease. In: Harris J. (eds) Protein Aggregation and Fibrillogenesis in Cerebral and Systemic Amyloid Disease. Subcellular Biochemistry, vol 65. Springer, Dordrecht
- [2] T. Vos et al., Global, regional, and national incidence, prevalence, and years lived with disability for 310 diseases and injuries, 1990-2015: a systematic analysis for the Global Burden of Disease Study 2015, *The Lancet*, vol. 388, no. 10053, pp. 1545-1602, Oct. 2016.
- [3] B. Peng, S. Wang, Z. Zhou, Y. Liu, B. Tong, T. Zhang, and Y. Dai, A multilevel-roi-features-based machine learning method for detection of morphometric biomarkers in parkinsons disease, *Neuroscience letters*, vol. 651, pp. 8894, 2017
- [4] H.-C. Cheng, C. M. Ulane, and R. E. Burke, Clinical progression in Parkinson disease and the neurobiology of axons, *Annals of Neurology*, vol. 67, no. 6, pp. 7157-725, Jun. 2010.
- [5] A. Sakalauskas, A. Lukoevicius, K. Lauckaite, D. Jegelevicius, and S. Rutkauskas, Automated segmentation of transcranial sonographic images in the diagnostics of parkinsons disease, *Ultrasonics*, vol. 53, no. 1, pp. 1111-121, 2013.]
- [6] B. Rana, A. Juneja, M. Saxena, S. Gudwani, S. S. Kumaran, R. Agrawal, and M. Behari, Regions-of-interest based automated diagnosis of parkinsons disease using t1-weighted mri, *Expert Systems with Applications*, vol. 42, no. 9, pp. 4506-4516, 2015.
- [7] D. Athauda et al., Exenatide once weekly versus placebo in Parkinsons disease: a randomised, double-blind, placebo-controlled trial, *The Lancet*, vol. 390, no. 10103, pp. 1664-1675, Oct. 2017.
- [8] N. K. Focke, G. Helms, S. Scheewe, P. M. Pantel, C. G. Bachmann, P. Dechent, J. Ebentheuer, A. Mohr, W. Paulus, C. Trenkwalder, Individual voxel-based subtype prediction can differentiate progressive supranuclear palsy from idiopathic parkinson syndrome and healthy controls, *Human Brain Mapping* 32 (11) (2011) 1905-1915.
- [9] S. Pazhanirajan and P. Dhanalakshmi, Classification of parkinsons disease using mri images, *International Journal of Computer Science and Software Engineering*, vol. 5, no. 10, p. 233, 2016
- [10] C. Salvatore, A. Cerasa, I. Castiglioni, F. Gallivanone, A. Augimeri, M. Lopez, G. Arabia, M. Morelli, M. Gilardi, and A. Quattrone, Machine learning on brain mri data for differential diagnosis of parkinsons disease and progressive supranuclear palsy, *Journal of Neuroscience Methods*, vol. 222, pp. 230-237, 2014.
- [11] H. Choi, S. Ha, H. J. Im, S. H. Paek, and D. S. Lee, Refining diagnosis of parkinsons disease with deep learning-based interpretation of dopamine transporter imaging, *NeuroImage: Clinical*, vol. 16, pp. 586-594, 2017.
- [12] G. S. Babu, S. Suresh, B. S. Mahanand, A novel PBL-McRBFN-RFE approach for identification of critical brain regions responsible for parkinson's 235 disease, *Expert Systems with Applications* 41 (2) (2014) 478-488.
- [13] S. Esmailzadeh, Y. Yang, and E. Adeli, End-to-end parkinson disease diagnosis using brain mr-images by 3d-cnn, *arXiv preprint arXiv:1806.05233*, 2018.
- [14] Diagnostic Imaging Dataset Statistical Release". Internet: <https://www.england.nhs.uk/statistics>, Oct. 27, 2016 [Aug. 10, 2018].
- [15] M. Buda, A. Maki, and M. A. Mazurowski, A systematic study of the class imbalance problem in convolutional neural networks, *Neural Networks*, vol. 106, pp. 249-259, Oct. 2018.
- [16] D. Long et al., Automatic Classification of Early Parkinsons Disease with Multi-Modal MR Imaging, *PLoS ONE*, vol. 7, no. 11, p. e47714, Nov. 2012.
- [17] H. Braak, K. Del Tredici, U. Rb, R. A. De Vos, E. N. J. Steur, and E. Braak, Staging of brain pathology related to sporadic parkinsons disease, *Neurobiology of aging*, vol. 24, no. 2, pp. 197-211, 2003.
- [18] B. Rana, A. Juneja, M. Saxena, S. Gudwani, S. S. Kumaran, M. Behari, R. K. Agrawal, Graph-theory-based spectral feature selection for computer aided diagnosis of parkinson's disease using t1-weighted MRI, *International Journal of Imaging Systems and Technology* 25 (3) (2015) 245-255.
- [19] B. Rana, A. Juneja, M. Saxena, S. Gudwani, S. S. Kumaran, M. Behari, R. Agrawal, Relevant 3d local binary pattern based features from fused feature descriptor for differential diagnosis of parkinsons disease using structural mri, *Biomedical Signal Processing and Control* 34 (2017) 134-143.
- [20] Parkinsons Progression Markers Initiative (PPMI), <https://www.ppmi-info.org/>, online; accessed 30 September 2019.
- [21] IXI Dataset, <https://brain-development.org/ixi-dataset/>, online; accessed 30 September 2019.
- [22] SPM, <https://www.fil.ion.ucl.ac.uk/spm/software/>, online; accessed 30 September 2019.
- [23] J. Ashburner, G. Barnes, C. Chen, J. Daunizeau, G. Flandin, K. Friston, S. Kiebel, J. Kilner, V. Litvak, R. Moran, et al., *Spm12 manual*, Wellcome Trust Centre for Neuroimaging, London, UK.
- [24] CAT A Computational Anatomy Toolbox for SPM, <http://www.neuro.uni-jena.de/>, online; accessed 30 September 2019.
- [25] M. W. Woolrich et al., Bayesian analysis of neuroimaging data in FSL, *NeuroImage*, vol. 45, no. 1, pp. S173-S186, Mar. 2009.
- [26] Y. Zhang, M. Brady, and S. Smith, Segmentation of brain MR images through a hidden Markov random field model and the expectation-maximization algorithm, *IEEE Transactions on Medical Imaging*, vol. 20, no. 1, pp. 455-7, 2001.
- [27] M. Jenkinson, M. Pechaud, and S. Smith. "BET2: MR-based estimation of brain, skull and scalp surfaces," In Eleventh Annual Meeting of the Organization for Human Brain Mapping, 2005
- [28] M. Jenkinson and S. Smith, A global optimisation method for robust affine registration of brain images, *Medical Image Analysis*, vol. 5, no. 2, pp. 143-156, Jun. 2001.
- [29] M. Jenkinson, P. Bannister, M. Brady, and S. Smith, Improved Optimization for the Robust and Accurate Linear Registration and Motion Correction of Brain Images, *NeuroImage*, vol. 17, no. 2, pp. 825-841, Oct. 2002.
- [30] J. Deng, W. Dong, R. Socher, L.-J. Li, K. Li and L. Fei-Fei, ImageNet: A Large-Scale Hierarchical Image Database, *CVPR09*. 2009.
- [31] Olga Russakovsky*, Jia Deng*, Hao Su, Jonathan Krause, Sanjeev Satheesh, Sean Ma, Zhiheng Huang, Andrej Karpathy, Aditya Khosla, Michael Bernstein, Alexander C. Berg and Li Fei-Fei. (* = equal contribution) ImageNet Large Scale Visual Recognition Challenge. *IJCV*, 2015.
- [32] J. Rieke, F. Eitel, M. Weygandt, J. Haynes, K. Ritter, Visualizing Convolutional Networks for MRI-based Diagnosis of Alzheimer's Disease, *Machine Learning in Clinical Neuroimaging (MLCN)*, 2018
- [33] Paszke, A., Gross, S., Massa, F., Lerer, A., Bradbury, J., Chanan, G., Killeen, T., Lin, Z., Gimelshein, N., Antiga, L., Desmaison, A., Kopf, A., Yang, E., DeVito, Z., Raison, M., Tejani, A., Chilamkurthy, S., Steiner, B., Fang, L., Bai, J., Chintala, S.: Pytorch: An imperative style, high-performance deep learning library. In Wallach, H., Larochelle, H., Beygelzimer, A., dAlch e-Buc, F., Fox, E., Garnett, R., eds.: *Advances in Neural Information Processing Systems* 32. Curran Associates, Inc. (2019) 8024-8035
- [34] Marcel S., Rodriguez, Y.: Torchvision the machine-vision package of torch. In: *Proceedings of the 18th ACM International Conference on Multimedia*. MM 10, New York, NY, USA, Association for Computing Machinery (2010) 1485-1488
- [35] Kornblith, Simon, Shlens, Jonathon, Le, Quoc. (2018). Do Better ImageNet Models Transfer Better?.
- [36] Mostafa, T.A., Cheng, I.: Parkinsons Disease Detection Using Ensemble Architecture From MR Images (2020)
- [37] George A. Miller (1995). *WordNet: A Lexical Database for English*. *Communications of the ACM* Vol. 38, No. 11: 39-41.
- [38] Christiane Fellbaum (1998, ed.) *WordNet: An Electronic Lexical Database*. Cambridge, MA: MIT Press.
- [39] He, K., Zhang, X., Ren, S., Sun, J.: Deep residual learning for image recognition. *arXiv preprint arXiv:1512.03385* (2015)
- [40] Iandola, F.N., Moskewicz, M.W., Ashraf, K., Han, S., Dally, W.J., Keutzer, K.: Squeezenet: Alexnet-level accuracy with 50x fewer parameters and 1mb model size. *arXiv:1602.07360* (2016)
- [41] Huang, G., Liu, Z., van der Maaten, L., Weinberger, K.Q.: Densely connected convolutional networks (2016)
- [42] Simonyan, K., Zisserman, A.: Very deep convolutional networks for large-scale image recognition (2014)
- [43] Sandler, M., Howard, A., Zhu, M., Zhmoginov, A., Chen, L.C.: *Mobilenetv2: Inverted residuals and linear bottlenecks* (2018)
- [44] Ma, N., Zhang, X., Zheng, H.T., Sun, J.: *Shufflenet v2: Practical guidelines for efficient cnn architecture design* (2018)